Journal of Catalysis 381 (2020) 615–625

Contents lists available at ScienceDirect

Journal of Catalysis

journal homepage: www.elsevier.com/locate/jcat

Utilization of hydrophobic ligands for water-insoluble Fe(II) water oxidation catalysts – Immobilization and characterization

Sahir M. Al-Zuraiji [a,b], Tímea Benkó [a], Levente Illés [c], Miklós Németh [a], Krisztina Frey [a], Attila Sulyok [c], József S. Pap [a,*]

[a] Surface Chemistry and Catalysis Department, Centre for Energy Research, Hungarian Academy of Sciences, H-1121, Konkoly-Thege Street 29-33, Budapest, Hungary
[b] Doctoral School on Materials Sciences and Technologies, Óbuda University, H-1034 Bécsi Street 96/b, Budapest, Hungary
[c] Institute of Technical Physics and Materials Science, Centre for Energy Research, Hungarian Academy of Sciences, H-1121, Konkoly-Thege Street 29-33, Budapest, Hungary

ARTICLE INFO

Article history:
Received 9 July 2019
Revised 12 November 2019
Accepted 1 December 2019
Available online 21 December 2019

Keywords:
Iron
Water oxidation
Molecular catalysis
Bidentate ligand
Heterogenization

ABSTRACT

Herein, we compare the electrochemical and electrocatalytic properties of two selected, water-insoluble Fe(II) coordination complexes made with the non-symmetric, bidentate ligands, 2-(2′-pyridyl)benzimidazole (PBI) in $[Fe(PBI)_3](OTf)_2$ (**1**, OTf^- = trifluoromethyl sulfonate anion) and 2-(2′-pyridyl)benzoxazole (PBO) in $[Fe(PBO)_2(OTf)_2]$ (**2**) . Cyclic voltammetry in water/acetonitrile mixture indicates considerable activity for both compounds. However, only **1** acts as homogeneous catalyst. The complexes have been successfully immobilized on indium-tin-oxide (ITO) electrode surface. The hydrophobic ligands allowed for a simple dip-coating and drop-casting of **1** and **2** onto ITO. Both **1**/ITO and **2**/ITO showed increased activity in electrocatalytic O_2 evolution in borate buffer at pH 8.3. According to scanning electron microscopy (SEM), energy dispersive X-ray spectroscopy (EDX), X-ray photoelectron spectroscopy (XPS), moreover, re-dissolution tests, the Fe remains in complex with PBI during electrolysis in the drop-casted, nano-porous films of **1**/ITO. In contrast, the PBO complex in **2**/ITO undergoes a rapid *in situ* decomposition yielding a mineralized form that is responsible for catalysis.

1. Introduction

Currently the world's energy supply is largely based on fossil fuels, which manifests in severe global problems, such as greenhouse effect, pollution, and energy crises. The development of sustainable energy systems is urgently required. The efficient utilization of sunlight to generate solar fuels draws considerable attention nowadays [1–6]. Hydrogen is among the most perspective chemical energy carriers that can be generated in a pure form by the splitting of water. The oxygen evolution reaction (OER), $2H_2O \rightarrow O_2 + 4H^+ + 4e^-$, is arguably the most challenging process of the overall water splitting. The removal of four protons and four electrons from two water molecules, which undergo O—O bond formation to produce O_2 as the final step, is a demanding process both from the kinetic and the thermodynamic point of view [7–9]. It has been demonstrated for several Ru- or Ir-based water oxidation catalysts (WOCs) that efficiency can be combined with robustness by molecular design [10,11]. On the other hand, it is clear that low-cost, robust and effective WOCs should rather rely on abundant elements. Fascinating new results on molecular catalysts based on V [12], Mn [13], Fe [14–22], Co [23,24], Ni [25,26] and Cu [27,28] indicate that fundamental research can be fruitful to advance the field in this direction. However, while high abundance and low cost of these metals are appealing properties, the often insufficient stability of their complexes remains a serious challenge [29].

A prominent representative of these metals is iron that is involved in a number of biochemical and artificial catalytic oxidation processes where $Fe^{IV/V}$=O active species proved to be responsible for the reactivity [29–33]. This fact is encouraging with respect to potential application of Fe in single-site molecular WOCs [34,35], since the high oxidation state M=O intermediate required for the water nucleophilic attack (WNA) should be available from Fe^{II}—OH_2 or Fe^{III}—OH/OH_2 complexes. Indeed, Collins and coworkers reported Fe-based WOCs by using fluorine-substituted tetraamidomacrocyclic (TAML) ancillary ligands (Fig. 1) and Ce^{IV} as the oxidant [17]. Recently, complexes with tetradentate N-donor ligands have been reported to outperform the TAML complexes [36]. Fillol, Costas *et al.* reported a range of Fe compounds with N_4-donor ligands that were able to catalyze the OER at low pH [15]. Subsequently, Codolà *et al.* designed several complexes

* Corresponding author.
E-mail address: pap.jozsef@energia.mta.hu (J.S. Pap).

https://doi.org/10.1016/j.jcat.2019.12.003
0021-9517/

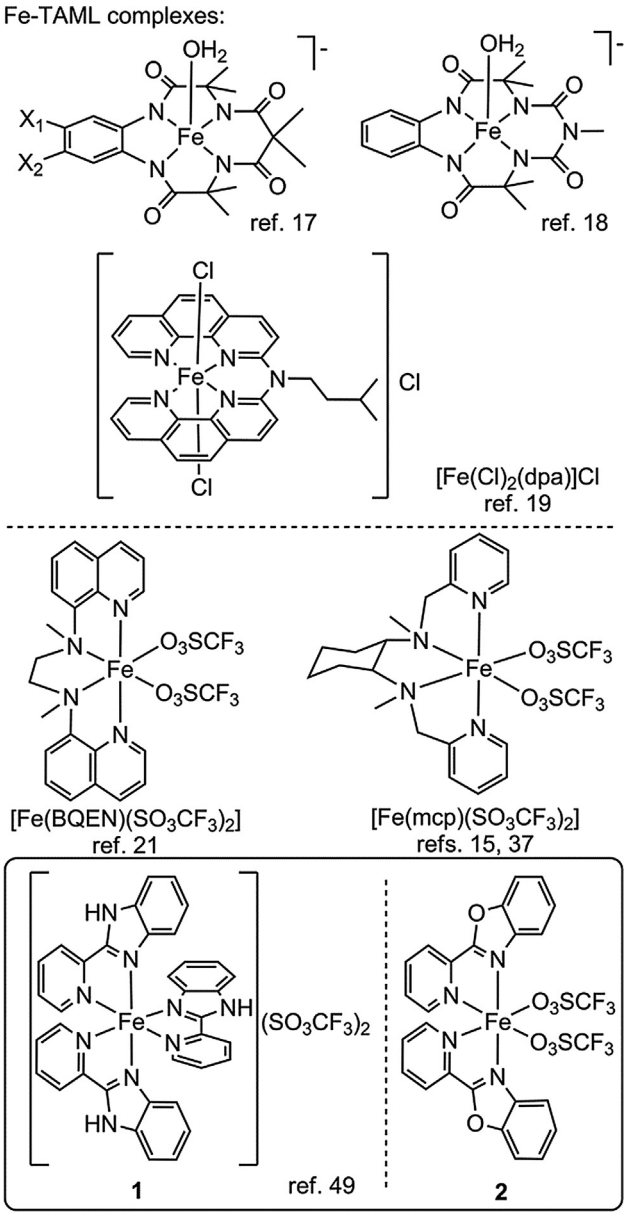

Fig. 1. Selected representatives of single-site molecular Fe catalysts for water oxidation and the complexes applied in this study.

(differing in their ligand topology) and explored their drastically different activities in acidic media [37]. While in the above examples Ce^{IV} was applied as sacrificial oxidant, Hetterscheid and coworkers did pioneering work on Fe complexes capable of electrocatalysis with various tetradentate ligands like cyclam, cyclamacetate [38] and *N,N*-bis(2,2-bipyrid-6-yl)amine [39].

Some shared features of the most active systems allow appointing further WOC candidates that is, the easy access to high oxidation states, robust ancillary ligands and *cis*-coordination of two water molecules (note that di- and multinuclear catalysts [14,19,40] are not considered here). In addition, complex decomposition under the working conditions may lead to another species or all the way to iron oxides [41]. In order to develop advanced systems involving Fe-based WOCs in (photo)electrocatalysis that can benefit from the advantages of these molecular units, their immobilization with semiconducting materials would be a next logical step.

Grafting molecules to the surface through bridging ligands typically requires one or more synthetic modification steps in the ancillary ligands to introduce anchoring groups [41,42]. A tailored assembly can be also achieved through self-assembly and surface precipitation of precursors for molecular electrocatalysts, immobilization *via* physical confinement, and electrostatic, non-covalent immobilization, especially by layer-by-layer (LbL) assembling methods [43]. One also needs to consider that a slight change in the reaction conditions may have a great effect on both the stability of WOCs and the operating mechanism [34,44–46].

As for Fe-based molecular WOCs, Shi *et al.* [47] demonstrated an inexpensive and convenient synthetic strategy of nanostructures prepared by unsubstituted iron(II) phthalocyanine/carbon nitride nanosheet (FePc/CN) nanocomposites, moreover, a TAML-based catalyst was also successfully immobilized by mixing with carbon black [48].

Herein we report the utilization of two selected coordination complexes with non-symmetric, readily available bidentate ligands, *i.e.*, 2-(2′-pyridyl)benzimidazole (PBI) in $[Fe(PBI)_3](OTf)_2$ (**1**, OTf^- = trifluoromethyl sulfonate anion) and 2-(2′-pyridyl) benzoxazole (PBO) in $[Fe(PBO)_2(OTf)_2]$ (**2**) [47] (Fig. 1). The ligands have been shown earlier to influence the reactivity against H_2O_2 in acetonitrile and, importantly, electrochemical and ^1H NMR evidence was presented in support of ligand exchange in the presence of trace (or added) water in the solution. In the present study we show that addition of water to acetonitrile leads to water oxidation electrocatalysis at high anodic potentials in the presence of **1** or **2**, but with marked differences. Experimental results suggest that Fe remains coordinated to the PBI ancillary ligand after the catalytic process, while the application of the weaker donor PBO leads eventually to the mineralization of the metal. It will be discussed herein that the water-insoluble ancillary ligands aid the immobilization of compounds **1** and **2** on indium tin oxide (ITO) electrode, but these ad-layers behave very differently under the conditions of electrocatalysis in aqueous buffer.

2. Experimental section

2.1. Materials synthesis

Solvents (acetonitrile, methanol, ethanol), Nafion solution in methanol, D_2O, and tetrabutylammonium perchlorate (TBAP) were purchased from commercial sources and used without further purification. $Fe(CF_3SO_3)_2$ was purchased from Strem Chemicals. The ligand 2-(2′-pyridyl)benzimidazole was purchased from Sigma-Aldrich, 2-(2′-pyridyl)benzoxazole, **1** and **2** were synthesized according to known procedures [49].

2.2. Physical characterization

Electrochemistry with homogeneous systems. Cyclic voltammetry (CV) and chronoamperometry (CA) were performed on a BioLogic SP-150 potentiostat. For kinetic experiments, the catalyst concentration was varied between 0.01 and 0.2 mM and water was added in 0–1.9 M concentration to acetonitrile. Experiments were conducted under Ar with a standard three-electrode setup including a boron-doped diamond (BDD) working electrode (polished and conditioned before each use), Pt auxiliary electrode and Ag^+/Ag (0.01 M $AgNO_3$, 0.1 M TBAP/acetonitrile) reference electrode. The plotted potentials were referenced against the ferrocenium/ferrocene (Fc^+/Fc) couple.

Deposition of the complexes on semiconductor (ITO). Indium tin oxide (ITO, ~100 nm thickness) coated glass slides were purchased from PGO, Germany. Two different procedures were applied:

A. *Dip-coating:* ITO coated glass slides (14 × 14 mm) were cleansed with ethanol in an ultrasonic bath for 20 min, then rinsed and dried. Complex **1** was dissolved in methanol with or without adding Nafion (5 wt% in water/methanol) to reach a final concentration of 0 or 0.4 wt% for Nafion and 0.4–6.0 mM for **1**. With complex **2** (0.4–10.0 mM) the concentration of Nafion was varied between 0 and 0.8 wt% to obtain different composite films. The ITO pieces were dipped into the coating solutions for 1 min, and then kept at room temperature for 30 min, finally heated for 30 min at 90–110 °C.

B. *Drop-casting:* Complexes **1** and **2** were dissolved in methanol in 6 mM concentration. Small portions of the solutions (50–150 μL) were evenly layered onto the cleansed ITO by using a micro-syringe. Methanol was evaporated at room temperature and after that, dried by an infrared lamp for 30 min (Fig. 2). The same procedure was replicated with the addition of Nafion to **1** in methanol to prepare **1**/Nafion/ITO composite films, but no significant difference was observed in comparison with **1**/ITO sample.

Electrochemistry with surface-deposited samples. All experiments were conducted in 0.2 M borate buffer (pH 8.3) under argon. An ITO piece layered with **1** or **2** (by method A, or B) was set as the working electrode in a three-electrode setup (Pt auxiliary and Ag/AgCl reference). The O_2 evolution was measured by either an optical probe (NeoFox) immersed into the electrolyte, or, by gas chromatographic analysis (Shimadzu GC 2010 Tracera equipped with a BID detector) of 200 μL samples from the headspace of the air-tight cell (in this case the cell was under air). The carrier and the plasma gas was 6.0 He. The in- and outlet pipes were connected to a home-made loop including an injector unit, a circulating micro-pump and a 4-stand valve to allow filling the loop with He gas. The samples were injected to this gas-tight loop and analyzed by GC. Calibration of the setup for sample volume and component sensitivity was done with the help of He gas and artificial air. The instrument settings were as follows: 50 mL/min total flow rate, 40 mL/min DCG flow rate, 3 mL/min purge flow rate, $T_{col.}$ = 35 °C, $T_{det.}$ = 250 °C.

Scanning electron microscopy (SEM) and energy dispersive X-ray spectroscopy (EDX). These investigations were done on a Thermo Scientific Scios2 dual beam system equipped with an Oxford X-max^n 20 SDD EDX, 5 keV beam energy and process time 6 were applied, dead time was below 50%.

X-Ray photoelectron spectroscopy (XPS). Surface compositions of the film deposited on the ITO electrode were determined by a KRATOS XSAM 800 XPS instrument equipped with an atmospheric reaction chamber. Al Kα characteristic X-ray line, 40 eV pass energy (energy steps 0.1 eV) and FAT mode were applied for recording the XPS lines of the Fe *2p* and *3p,* O *1s,* Sn *3d,* In *3d,* N *1s*, C *1s*, B *1s*, F *1s,* S *2p* and Na *1s* photoelectrons, and the C *1s* binding energy at 284.8 eV was used as reference for charge compensation. The surface ratios of the elements were calculated from the integral intensities of the XPS lines using sensitivity factors given by the manufacturer.

UV–visible spectrophotometry. Absorption spectra were recorded on an Agilent Cary 60 spectrophotometer with 0.2 cm path length quartz cuvette at 25 °C.

Fig. 2. Typical drop-casted samples of **1**/ITO (left, for CPE) and **2**/ITO (right, for CV).

3. Results and discussion

3.1. Redox properties of the complexes in homogeneous water/acetonitrile mixtures

It has been reported earlier that the non-symmetrical NN' ligands react spontaneously with Fe(II) triflate in dry acetonitrile under inert atmosphere. With PBI the red *tris*-chelate complex **1**, while with PBO the neutral, orange *bis*-chelate complex **2** is formed (Fig. 1). Complex **1** shows Fe—N bond lengths typical for low spin complexes (~2.0 Å), while **2** is high spin, exhibiting Fe—N bond lengths above 2.15 Å according to single crystal structural analyses [49,50]. We synthesized these compounds according to the reported procedures and obtained similar yields of the spectroscopically confirmed crystalline products.

According to the planned utilization of the complexes in water oxidation, we first investigated their redox behavior in acetonitrile without (Fig. 3) or with added water (Figs. 4 and S1) to trace the expected ligand exchange reactions. Our findings corroborate with the earlier observations, that are, even trace amounts of water (*i.e.*, some equivalents typically present in acetonitrile stored under air) cause a cathodic shift in the oxidation potential and irreversibility of the otherwise quasi-reversible Fe(III)/Fe(II) redox couple characteristic for **1** [49]. Importantly, it has been also pointed out earlier that complex **1** in acetonitrile exhibits paramagnetically broadened ^{1}H NMR spectrum typical of high spin Fe(II) complexes, which is indicative of rapid ligand exchange with trace amount of water present. As a consequence we observed this oxidation at *ca.* + 0.4 V *vs.* Fc^+/Fc (Fig. 4, inset), and the addition of water caused further cathodic shift in its potential (Fig. 4 inset, indicated with blue arrow).

This indicates the preference of Fe(III) for two aqua over N-donor ligands in accordance with the strikingly similar behavior of other Fe(II) complexes containing N_4 ligands [51]. In **1**, the

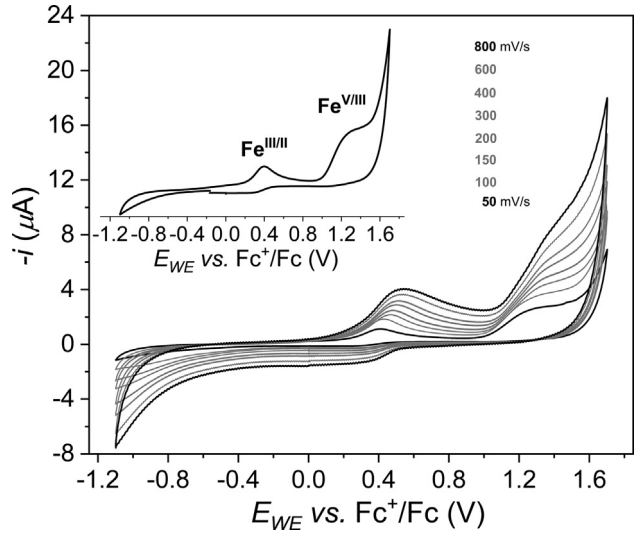

Fig. 3. Cyclic voltammograms of **1** (0.04 mM) in acetonitrile (0.1 M TBAP, BDD working electrode, 25 °C, under Ar) at scan rates as indicated. Inset: magnified view of the 50 mV/s CV curve with the proposed peak assignments.

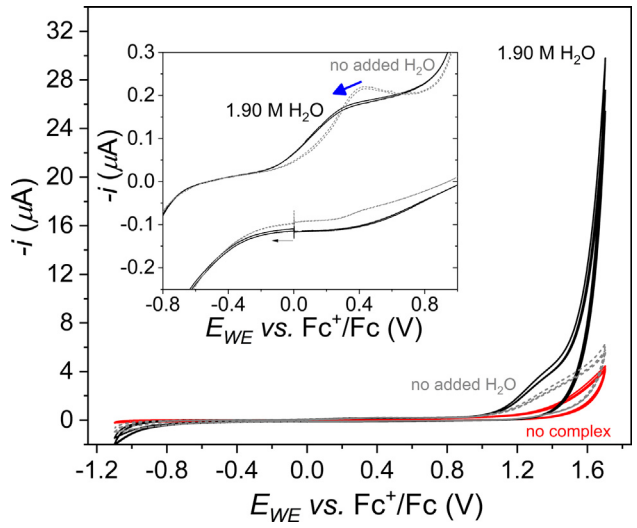

Fig. 4. Cyclic voltammetry of **1** in acetonitrile with no added water (0.01 mM, 0.1 M TBAP, grey curve), in the presence of added H_2O (1.90 M, black curve), and when no complex is present, but water is added (1.90 M, red curve), at ν = 100 mV/s, BDD working electrode, 25 °C, under Ar. Inset: blown up view of the potential range, where the Fe(III)/Fe(II) transition undergoes cathodic shift (blue arrow) upon the addition of H_2O.

configuration of the PBI ligands is expectedly *OC*-6-21 (*mer*) as indicated by the structure of the homolog low spin Fe(II) complex with 2-(2′-pyridyl) -*N*-methylbenzimidazole (MePBI) [49] and that of the $[Fe^{II}(PBI)_3](ClO_4)_2{\cdot}CH_3CN{\cdot}H_2O$ [50]. We infer that water molecules induce the dissociation of a PBI ligand and occupy the two available sites in *cis*-positions thus upon electrochemical oxidation to Fe(III) (Scheme 1), a preferred arrangement for efficient water oxidation catalysis can be achieved (note that ligand exchange has been evidenced viable in the presence H_2O_2, or *para*-substituted pyridine ligands [49]).

Further anodic scanning yields an irreversible wave of larger amplitude that is present at roughly +1.25 V *vs.* Fc^+/Fc (Fig. 3, inset). Notice that $[Fe^{IV}(N4Py)(O)]^{2+}$ (containing the neutral pentadentate ligand N4Py) was successfully generated by bulk electrolysis in water/acetonitrile at similar potential (> +1.3 V *vs.* Fc^+/Fc) starting from $[Fe(N4Py)(CH_3CN)_2]^{2+}$ [52]. The Fe(III) to Fe(IV) oxidation seems to be a valid assignment in our case, too, which would provide $[(PBI)_2Fe^{IV}(OH_2)(O)]^{2+}$. Since there is no other visible oxidation peak between the catalytically enhanced current (see below) and this oxidation of the complex, the Fe(III) to Fe (IV) assignment would mean that the latter is responsible for the catalysis. However, in similar complexes to ours, which bear neutral N4 ligands and allow *cis*-diaquo coordination, the $(L^{N4})Fe^{IV}(OH_2)(O)$ motif was associated with the resting state in the Ce^{IV} excess-driven catalytic cycle [16,37,53,54]. This form yielded $(L^{N4})Fe^{V}(O)(OH)$ through PCET for which the potential was calculated to be roughly +1.7 V *vs.* NHE at pH 1 by computational methods [54] and the Fe(V) species was suggested to participate in water nucleophilic attack. Based on these facts, moreover, the 2.3-times higher current passed at +1.25 V than at +0.4 V (Fig. 3, inset, the scan rate is 50 mV/s) indicating a 2-electron, or two energetically leveled 1-electron transitions we tentatively assign this oxidation event to the generation of a $[(PBI)_2Fe^{V}(OH)(O)]^{2+}$ (**1a**^{ox}) species stabilized by the negatively charged *cis*-ligand (Scheme 1). Importantly, high excess of water to **1** drastically enhances the current above the potential where **1a**^{ox} is generated over several CV scans indicating an electrocatalytic event (Fig. 4) that should therefore involve water molecules and **1a**^{ox}. We further evidenced this

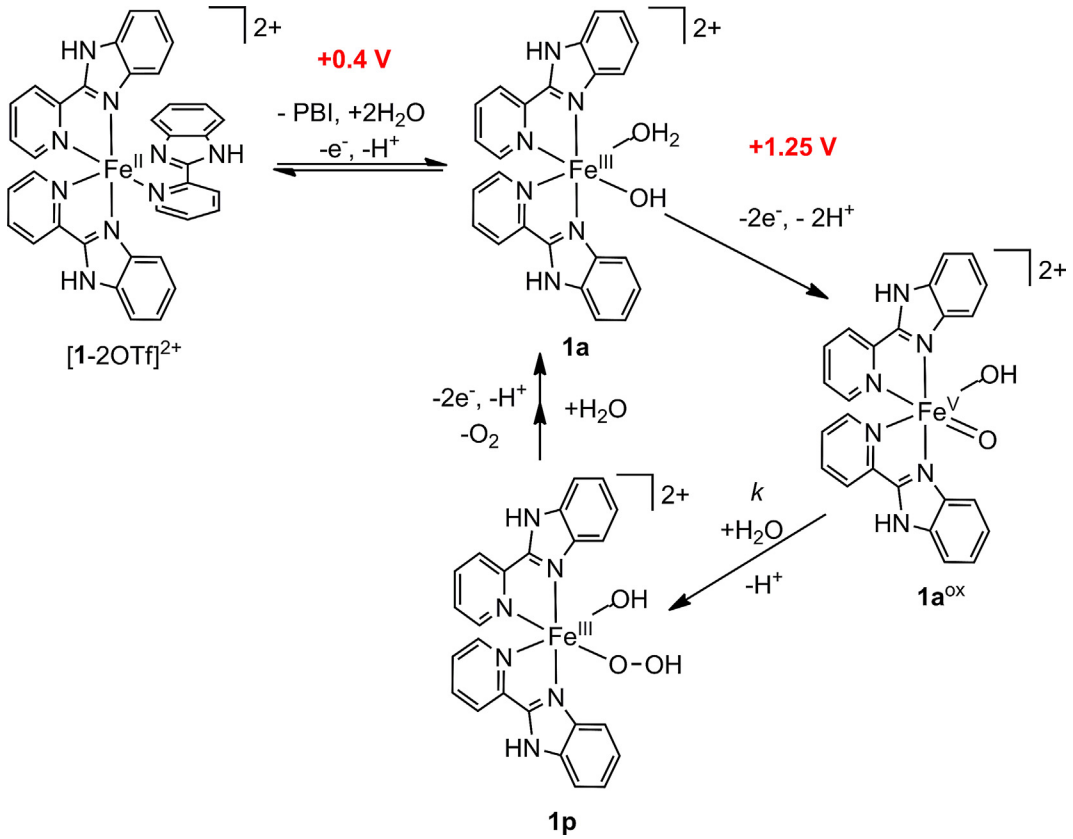

Scheme 1. Proposed mechanism for molecular water oxidation with complex **1a** (potentials are *vs.* the Fc+/Fc couple).

assumption by investigating the concentration dependence in water and **1** (see also the oxygen evolution measurements by using the heterogenized complex in the next section).

The excess current over +1.2 V *vs.* Fc^+/Fc is proportional to the concentration of the complex (Fig. 5). In comparison, when only water is present the current in this potential range is negligibly low as shown by the CV curves in red in Figs. 4 and 5 (the same applies to the free ligand, too). Above roughly 0.05 mM concentration of **1**, saturation occurs in the current that is generally associated with substrate depletion near the electrode surface [55]. The square of the current at +1.7 V *vs.* Fc^+/Fc (i_{cat}^2) shows linear dependence on the water concentration upon its variation (Fig. 6). The dependence of i_{cat} on **[1]** and $[H_2O]$ is in line with the rate law in Eq. (1) considering the proposed mechanism in Scheme 1, since $[\mathbf{1a^{ox}}]$ should correlate with the initially added **1**. The expression of i_{cat} by Eq. (2) that applies under pure kinetic control (*e.g.*, in the scanned exponential growth region of i_{cat}) explains why the linear dependence of i_{cat}^2 on $[H_2O]$ as plotted in Fig. 6 indicates first order in the water substrate. This suggests participation of a bulk water molecule in the rate limiting step that can be considered as a bimolecular reaction between $\mathbf{1a}^{ox}$ and H_2O.

$$reaction\ \ rate = k_{cat}\left[\mathbf{1a}^{ox}\right] = k\left[\mathbf{1a}^{ox}\right][H_2O] \quad (1)$$

$$i_{cat} = nFA[1](k_{cat}D_1)^{0.5} = nFA[1](k[H_2O]D_1)^{0.5} \quad (2)$$

In Eqs. (1) and (2), k_{cat} is the catalytic rate constant (s^{-1}), k is the second order rate constant for the reaction between $\mathbf{1a}^{ox}$ and H_2O ($M^{-1}\ s^{-1}$), n is the number of electrons transferred (for water oxidation $n = 4$), F is the Faraday constant, A is the geometric area of the working electrode (cm^2), and D_1 is the diffusion coefficient of the catalyst ($cm^2\ s^{-1}$). This rate law suggests a single site mechanism for water oxidation like it was proposed for the iron complexes of general formula $[Fe(X)_2(L^{N4})]$ [15,16,37,53,54], or $[Fe^{III}(dpaq)(H_2O)]^{2+}$ with a pentadentate N-donor ligand [56].

By performing the CV experiment with deuterium oxide a kinetic isotope effect (KIE = $i_{cat}^2(H_2O)\ /i_{cat}^2(D_2O) = k_{cat}(H_2O)/k_{cat}(D_2O)$) of 2.0 can be calculated (Fig. S2) that is consistent with a rate limiting, multiple-site electron–proton transfer (MS-EPT) step, possibly with bulk water as the proton acceptor [57]. Notably, in contrast to our observations an apparent lack of KIE was concluded for catalysts that were activated by Ce^{IV} as terminal oxidant

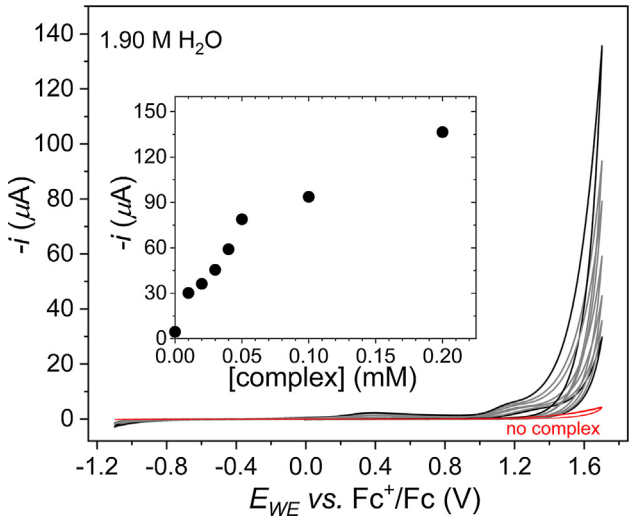

Fig. 5. Cyclic voltammetry of **1** (0.01–0.2 mM) in acetonitrile (0.1 M TBAP), in the presence of 1.9 M added water, v = 100 mV/s, BDD working electrode, Pt aux. electrode and non-aqueous Ag^+/Ag ref. el. Inset: currents at +1.7 V *vs.* Fc^+/Fc plotted against the catalyst concentration.

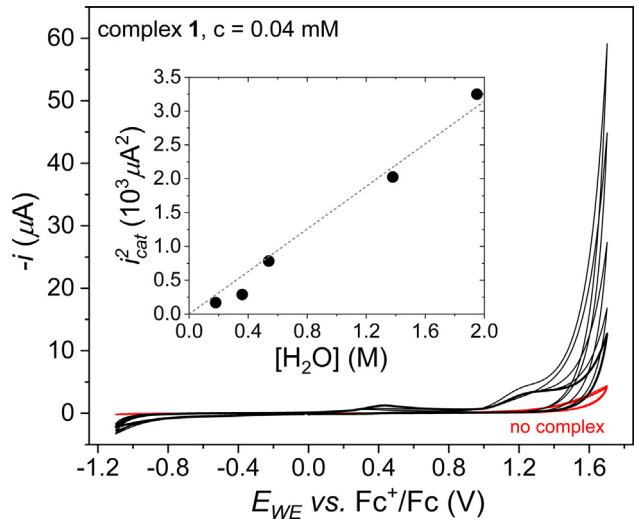

Fig. 6. Cyclic voltammograms of **1** (0.04 mM) in acetonitrile (0.1 M TBAP) with different amounts of added water and, when no complex is added (red curve), v = 100 mV/s, BDD working electrode, Pt aux. electrode and non-aqueous Ag^+/Ag ref. el. Inset: square of the currents at +1.7 V *vs.* Fc^+/Fc, plotted against of added water.

[53]. In a number of analog systems bearing N4 ligands an $Fe^{IV}(O)(\mu\text{-}O)\text{–}Ce^{IV}$ core was evidenced in the resting state adduct, which produced $Fe^{V}(O)(OH)$ following an inner sphere electron transfer mechanism [16,37]. According to the suggested mechanism this species reacts with H_2O in the rate-determining step providing $Fe^{III}(OOH)(OH_2)$ and only a minor reorganization of the O—H bonds takes place consistent with the lack of KIE [53].

On the basis of the experimental observations it is reasonable to propose that the attack of a water molecule at the oxo-ligand results in intermediate **1p** (Scheme 1), most likely assisted by a hydrogen-bond interaction with the second, hydroxide ligand of $\mathbf{1a}^{ox}$. Based on detailed computational work, the possible role of the adjacent hydroxyl ligand in binding and orienting the incoming water molecule has been previously discussed by Lloret-Fillol *et al.* [54]. Following the rate limiting step, the further oxidation of **1p** is proposed to affect the peroxide ligand resulting in facile O_2 release and H_2O coordination that means re-entering the catalytic cycle by re-forming **1a**. Notice that **1** was shown to react with H_2O_2 to give a green product identified as a μ-peroxido-diiron(III) species with considerable lifetime at room temperature. Its oxidation potential was more positive by *ca.* 0.4 V than that of **1** [49], which means that it is lower by roughly 0.6 V than the onset potential of the catalytic process. This observation supports that a proposed peroxide species resulting from the O—O bond formation step should undergo rapid oxidation during electrocatalysis due to the very high thermodynamic driving force.

It is to be mentioned here that returning to the ferrous state is unlikely during electrocatalysis and accordingly, the proposed mechanism involves **1a** as the resting state. As it will be discussed later, we detected Fe(III) on the surface of immobilized samples by X-ray photoelectron spectroscopy. In addition, successful re-dissolution tests in acetonitrile on used samples together with the CV and UV–vis results indicated that the molecular nature of the ad-layer is preserved. However, in the re-dissolved sample the intensity of the MLCT band associated with **1** was lowered that may be associated with the occurrence of Fe(III), too. On the other hand, the addition of ligand to the re-dissolved sample evidenced some reversibility toward re-forming **1**. By assuming, that in the immobilized layer only a part of the solid **1** is exposed to the polarization that is necessary to trigger catalysis, while another part remains aqua-coordinated Fe(II) that is capable of accepting the

added PBI this experimental finding supports the possibility of ligand exchange with water molecules as indicated by ^{1}H NMR and CV results.

In contrast to **1**, the Fe(III)/Fe(II) redox couple of **2** is irreversible and occurs at +0.75 V *vs*. Fc^+/Fc (Fig. 7, dashed CV curve, inset) that has been associated with the electron withdrawing nature of O compared with NH in the corresponding ligands [49]. This oxidation is followed by another one at +1.16 V *vs*. Fc^+/Fc that can be tentatively associated with an oxidation to the Fe(IV) or Fe(V) state. Single crystal structure of complex **2** confirmed *OC*-6-33 configuration of the donor atoms as shown in Fig. 1, and Fe—N(O) bond distances longer than 2.15 Å in the solid state that is typical of high spin Fe(II) complexes. The two triflate ligands are readily available for the exchange with water molecules (or acetonitrile in the absence of water), moreover, the high spin Fe(II) center should be unstable towards hydrolysis.

Upon the addition of water to the solution of **2** high anodic current occurs indicative of a catalytic event (Figs. 7 and S1). However, the current drops drastically from one cycle to another and the overall landscape changes completely in the low current regime, too (Fig. S1). If the cycling is started to the cathodic direction, the original peaks for **2** in acetonitrile cannot be observed anymore, instead, non-diffusion controlled currents are detected. This indicates that the high spin complex **2** is unstable and may hydrolyze in the presence of water. Indeed, in samples with added water slow precipitation of a fine solid product occurred. Also, after passing through the positive potentials re-dissolution peaks occur at *ca*. + 1.1 and −0.2 V *vs*. Fc^+/Fc that can be rendered decomposition products at the surface. After 10 cycles no more changes take place and two current peaks can be detected at +0.4 and +0.9 V *vs*. Fc^+/Fc, besides the catalytic current. Due to the complexity of the processes we did not attempt to explain the chain of events in more details. However, it is clear that the processes cannot be regarded as homogeneous, especially considering the results from the immobilized samples of **2** as it will be presented below.

In spite of the analog structure and NN' binding mode of the PBI and PBO ligands, the behavior of the two complexes under water oxidation conditions is strikingly different. We associate this difference with the electron withdrawing nature of O in PBO compared with NH in PBI, which makes PBI a stronger donor (as also reflected in the respective high *vs*. low spin electron configuration of the isolated Fe(II) complexes). Specifically, a supposed $[(PBO)_2$-$Fe^{III}(OH_2)(OH)]^{2+}$ and further oxidation products from **2** are expectedly degradation-prone due to the weaker donor PBO, which would be a plausible explanation for the non-homogeneous behavior in water/acetonitrile, moreover, for the mineralization of the deposited complex on the ITO surface (see below).

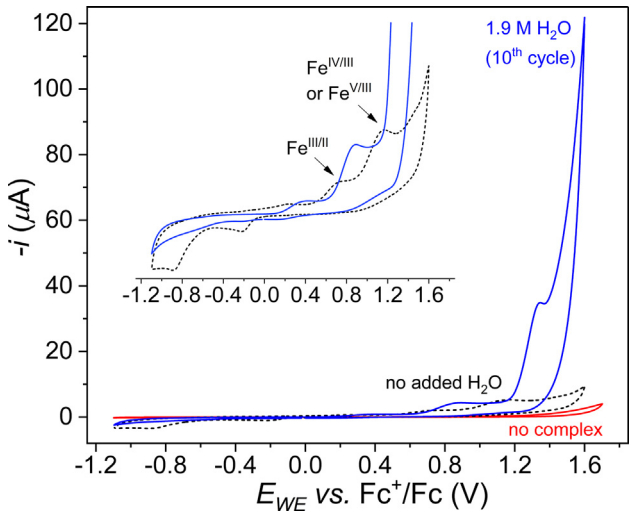

Fig. 7. Cyclic voltammetry of **2** (0.08 mM) in acetonitrile (0.1 M TBAP), in the presence or absence of 1.9 M H_2O and, when no complex is added (red curve), v = 100 mV/s (BDD working electrode, 25 °C, under Ar).

3.2. Deposited complexes on ITO

Complexes **1** and **2** are water insoluble thanks to the ancillary bidentate ligands. We hypothesized that hydrophobic interactions would keep the surface-deposited complexes on the ITO electrode during electrolysis in aqueous buffer. Also, it was presumed that the ligand exchange reactions observed in water/acetonitrile mixtures would take place at the solid–liquid interface upon contact of the layered ITO with the aqueous phase and this would allow carrying forward the catalytic activity of the molecular units.

We followed simple and scalable methods to graft **1** or **2** onto ITO-coated glass. According to the first procedure ITO pieces are dipped into methanol solutions of the complexes. With this method thin layers are expected upon drying. The performance of the modified electrode pieces is compared to the ITO in borate buffer at pH 8.3. CV shows increased currents over +1.2 V *vs*. Ag/AgCl as the concentration of **1** is increased in the dip-coating solution (Fig. S3). The same trend is observed in chronoamperometry (CA) currents at +1.4 V *vs*. Ag/AgCl (Fig. S3b). However, addition of Nafion (as support) has no significant effect on the steady currents. In the case of **2** the concentration of the dip-coating solution has no effect on the catalytic current (Fig. S4). Importantly, under identical conditions, both in CV and CA experiments the current is very low on plain ITO (Figs. S4 and S6). Although these experiments demonstrate the successful addition of the complexes as modifiers to ITO, the solubility of the complexes in methanol means an upper limit to the layer, moreover, at high concentration the ad-layer shows patchy distribution on the surface.

Drop-casting on the other hand is a rather controllable and convenient way to fabricate **1**/ITO and **2**/ITO (Fig. 2) that can be tested for longer periods of CA. In this case the volume of the drop-casted solution of **1** or **2** in methanol can be adjusted to yield different surface concentration of the corresponding complex. For a series of **1**/ITO CV currents increase proportionally as the amount of the complex is changed from 0.26 to 0.78 μmol on a 1.56(14) cm^2 ITO surface (Fig. 8a). Over multiple CV scans (apart from an initial drop) the current is unchanged indicating the presence of an electrochemically activated proportion of the catalyst derived from **1** under the conditions of the experiment. The oxidation peak at +0.8 V *vs*. Ag/AgCl can be assigned as the Fe(III)/Fe(II) transition of this form that is followed by a catalytically enhanced Faraday current with an onset potential of +1.2 V (similar characteristics were observed in the water/acetonitrile solution). On the reverse scan a reduction can be observed at +0.02 V *vs*. Ag/AgCl that can be associated with the coordination of water molecules. The nearly 800 mV separation from the Fe(III)/Fe(II) oxidation may originate from the increased stability of the Fe(III) state in the presence of aqua ligands. The low reversibility on both sides suggests rapid ligand exchange, resulting in an electrochemical-chemical-electro chemical (ECE) mechanism. Notice that upon cathodic polarization, when the complex is reduced to the Fe(II) state there is enough driving force for the aqua ligands to dissociate from the complex. However, it is uncertain, which potential ligands compete for the empty sites.

The overpotential calculated from the 5th CV scan ($\eta = E_{WE} + E$ (Ag/AgCl) – $E°(O_2/H_2O)$ + 0.059pH, no *i*R compensation) at j = – 0.1 mA/cm^2 is +0.78 V and the Tafel slope is 241(2) mV/dec (Fig. 8b) that signals considerable kinetic barrier for the catalysis.

Controlled potential electrolysis (CPE) experiments were performed at +1.2 V *vs*. Ag/AgCl in a different cell, where the compart-

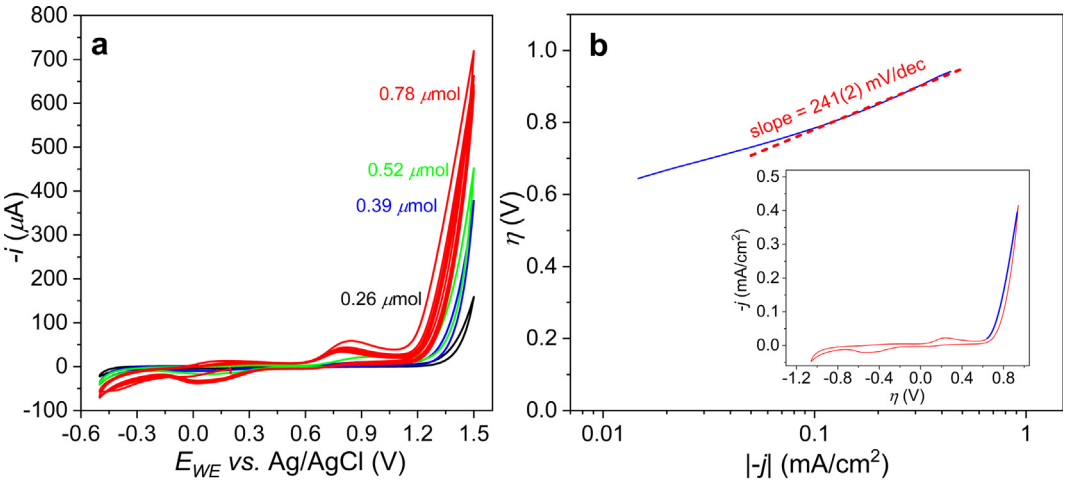

Fig. 8. (a) Cyclic voltammetry of drop-casted **1**/ITO in 0.2 M borate buffer (pH 8.3, v = 100 mV/s, Pt aux. separated with Vycor frit and Ag/AgCl ref. electrode); (b) Tafel plotting from the blue segment of the 5th CV scan, which is shown in the inset).

ment of the counter electrode was separated by Nafion membrane. The almost instant O_2 evolution could be confirmed with an optical oxygen sensor immersed near the **1**/ITO surface (Fig. S5). During the first 15 min the evolved O_2 corresponds to the passed charge with ~100% Faraday efficiency and the color of the layer changes from brick-red to wine-red (Fig. 10, inset). After saturating the electrolyte the evolved gas diffuses out from the solution causing an apparent decline from the [O_2] calculated for 100% Faraday efficiency. However, the current remains steady for over 2 h, during which time ~6 C (corresponds to 62.2 μmol of electrons) passes (Fig. 9) and bubble formation is continuous. Plain ITO gives negligible current under identical conditions (Fig. 9). The oxygen evolution was also confirmed and quantified by gas chromatography analysis of a headspace sample after 100 min of electrolysis at +1.4 V *vs.* Ag/AgCl (Fig. S6). Notice that in this experiment 0.52 μmol of **1** has been spread over ~1.68 cm^2 of which ~1.5 cm^2 was immersed into the solution, thus roughly 0.46 μmoles of **1** was in contact with the electrolyte. After passing 13.22 C of charge (corresponding to 137 μmoles of electrons, or 34.25 μmol O_2) 33.4 μmol O_2 could be detected by GC. This means an overall turnover number (TON) of 73 within 100 min by 98% Faraday efficiency at η = 0.86 V, corresponding to a TOF of 0.012 s^{-1} based on the detected product.

The surface morphology of a freshly prepared **1**/ITO electrode and after use in electrolysis for 2 h at +1.2 V *vs.* Ag/AgCl was analyzed by scanning electron microscopy (SEM) (inset pictures in Fig. 10a and 10b, respectively). The composition was analyzed both by energy dispersive X-ray spectroscopy (EDX, Fig. 10a and 10b, respectively) and X-ray photoelectron spectroscopy (Tables S1 and S2, Figs. S7 and S8).

The surface morphology of the freshly prepared **1**/ITO (Fig. 10a, insets) shows cracks in the layer, but otherwise the surface is relatively featureless, *e.g.*, no smaller pores can be seen. The elemental composition by EDX reflects the expected C, N and Fe for the complex cation and the F, O and S from the triflate counter ion (Fig. 10). The color of the complex exposed to CPE becomes darker (Fig. 10b, inset). A similar color change was observed by others for the low spin $[Fe(phen)_3](NCS)_2$ after its transformation to the high spin $[Fe(phen)_2(NCS)_2]$ in the solid phase [58]. In the case of **1** the color change may also indicate ligand exchange that would be consistent with the formation of **1a**. The surface of the layer is cracked and the layer structure is porous with pore sizes in the 100 nm

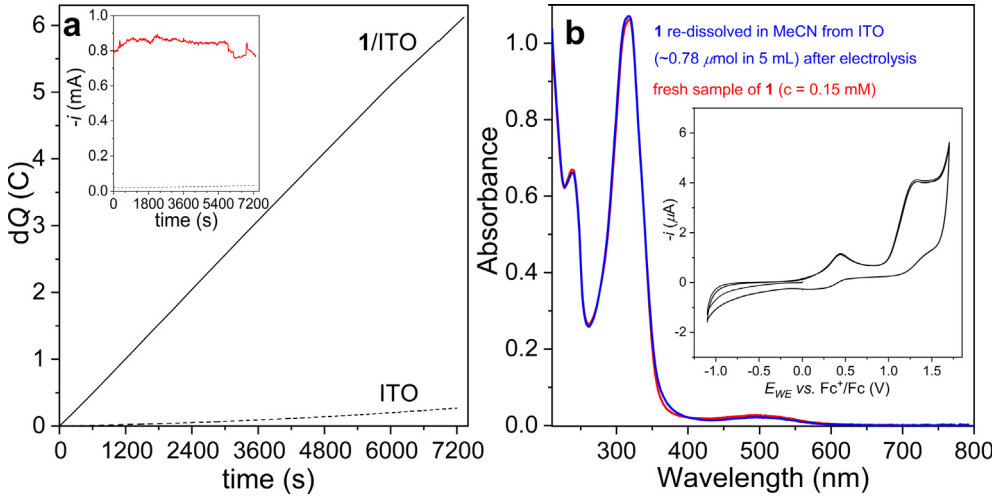

Fig. 9. (a) The passed charge during controlled potential electrolysis with **1**/ITO and plain ITO (dashed line) at +1.2 V *vs.* Ag/AgCl for 2 h in 0.2 M borate buffer, at pH 8.3. The inset shows the corresponding current *vs.* time plot; (b) UV–vis spectrum of the solid re-dissolved in acetonitrile from **1**/ITO after electrolysis and comparison to a fresh sample of **1**. Inset: cyclic voltammetry with the same re-dissolved sample.

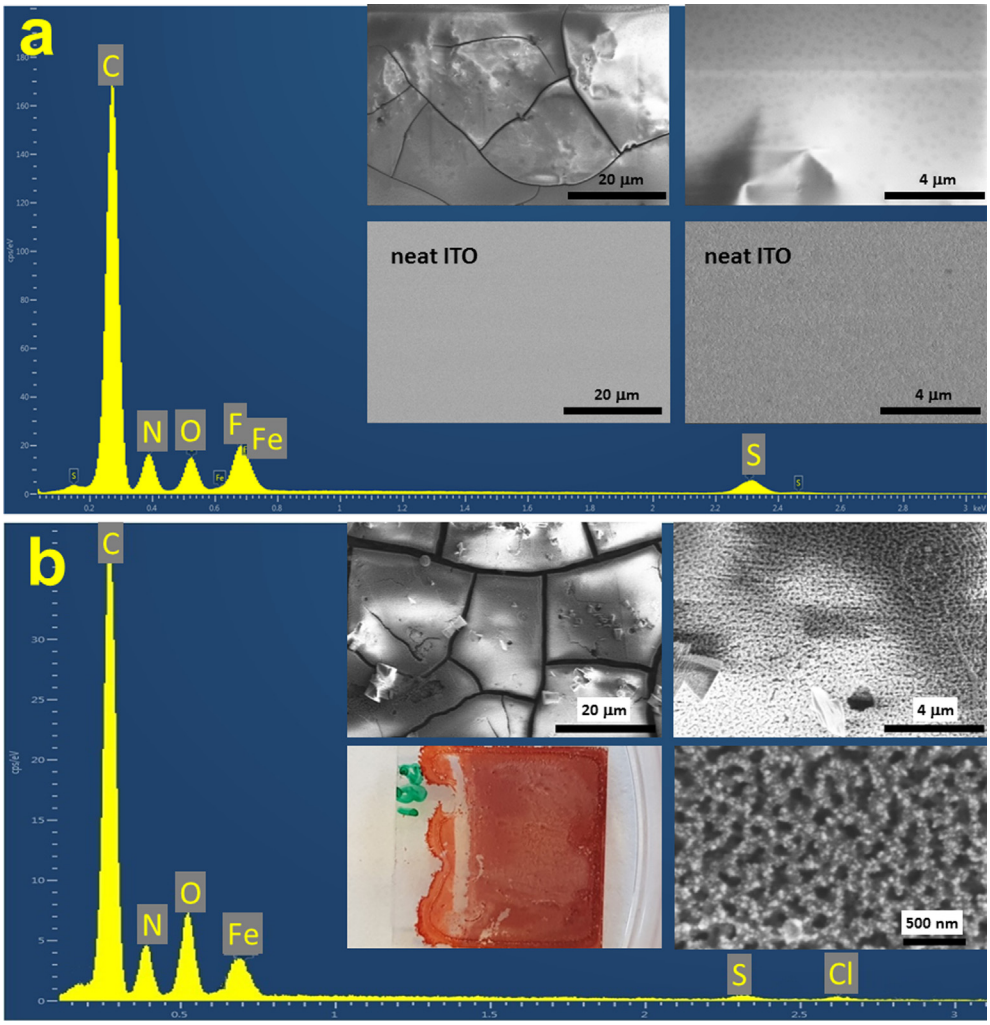

Fig. 10. (a) EDX spectrum of a freshly prepared **1**/ITO sample, inset: SEM pictures of the sample and the neat ITO surface at × 2000 and × 10,000 magnification; (b) EDX spectrum of **1**/ITO after electrolysis (for experimental details see Fig. 9), inset: photo and SEM pictures of the used electrode at ×2000, ×10,000 and ×50,000 magnifications. Experimental conditions for SEM: 2 kV beam accelerating voltage, 0.10 nA probe current, Everhart-Thornley detector, operation for secondary electron, 6.4 mm working distance. The detection mode was optimized for horizontal plane with short working distance.

range. This porous structure may be responsible for the high durability and good catalytic performance of the deposit, since it helps channeling O_2 bubbles from the surface.

The C, N, Fe, O, S major components in the EDX spectrum (Fig. 10b) are consistent with the elementary constitution of the complex. Two major differences may be highlighted. The O content has increased, which is reasonable regarding that the sample has been exposed to water for a long period of time, moreover, it is also consistent with the occurrence of the proposed **1a** form. The second difference is the lowered F and S content, which indicates that upon electrolysis the triflate is partly dissolved.

A more detailed analysis of the used **1**/ITO was done by XPS that revealed the presence of Fe, C, N, O, S and F in the surface layer (Fig. S7), beside Sn and In, in qualitative agreement with the elemental composition of **1a**. In comparison with the surface composition of the as-prepared **1**/ITO, the O/Fe ratio is higher, while the N and C content is lower in the used sample (Table S1). The calculated surface composition for the used sample is Fe/C/N = 1/20.6/3.8 (Table S1, for **1a** with two ancillary ligands 1/(2 × 12)/(2 × 3) would be expected), thus indicates that the surface is enriched in iron. This also stands for the as-prepared sample suggesting that the immediate surface layer contains a complex form with equal PBI to Fe ratio. This is probably a minor accompanying equilibrium form that is layered on **1** upon drying from its methanol solution.

The Fe(2p) peaks do not exhibit apparent satellite features that would be revealing on the high spin state. However, the peaks are broad and somewhat asymmetric, moreover, the splitting between them, Δ = Fe($2p_{3/2}$) – Fe($2p_{1/2}$) = 13.9 eV (Fig. S8, for data see Table S2) falls in the range reported for high spin complexes with increased spin-orbit coupling, for example [Fe(phen)$_2$(NCS)$_2$] that has been examined as a powder on ITO support [58], or other spin-crossover complexes [59,60]. In conclusion, we believe that Fe(III) is found in the surface layer. Interestingly, the as-prepared sample shows features for the surface Fe-content (Tables S2) that also suggest Fe(III) in considerable proportion. However, the Δ value is lower (13.7 eV) and the Fe(II) content is ~40%. As a consequence, in the case of this immobilized system the presence of Fe (III) cannot be associated with only **1a** to the analogy with the proposed homogeneous catalytic cycle.

The detailed analysis of the N 1s peak in the used sample tells about the Fe-N interaction. The ancillary ligand PBI contains N atoms in two environments, *i.e.*, a non-coordinated NH heterocyclic group (N_{hc}) and two coordinated (Fe—N_{hc}) donor groups in 2:1 ratio. Indeed, fitting of the N 1s peak reveals two components at 399.5 and 397.8 eV binding energy in ~2:1 ratio (Fig. S8). The com-

ponent at higher binding energy can be associated with the coordinated N donor atoms, while the component at lower binding energy with the non-coordinated N_{hc} atoms. This is consistent with the fact that the electron density shared in the dative bond is expected to increase the binding energy of the 2p electrons.

On the basis of these findings one can surmise that the upper layer of the complex coating detected by XPS consists of an iron (III) complex form that has higher iron content than that of **1a**, possibly exhibiting only one PBI ligand per Fe. Since XPS informs only about the upper proportion of the layer (which should be separated from the ITO electrode), the contribution of this component to the catalysis is hard to judge, but it cannot be excluded.

After surface analysis the drop-casted layer of **1** was easily re-dissolved in acetonitrile and its UV–vis absorption spectrum fits well with that of a freshly prepared solution of **1** (Fig. 9b). The intra-ligand charge transfer band at 316 nm is identical to that of the fresh sample, showing no sign of ligand degradation or considerable dissolution during electrolysis. The metal-to-ligand charge transfer (MLCT) band at 497 nm is also present, but it is lowered by 19% in intensity. This might be attributed in part to metal ion loss upon electrocatalysis, but it is more likely that some of the complex is present in a high spin $[Fe(PBI)_2(X)_2]^{2+}$ form, where X is solvent ligand, exhibiting no MLCT band. Likewise, it cannot be ruled out that some of the complex is in the ferric state that would be in accordance with the XPS findings. In the original complex the iron(II) center is surrounded by three ligands. However, during water oxidation one of the ligands is proposed to be exerted. UV–vis measurements in acetonitrile with added ligand to a re-dissolved sample (used in electrolysis at +1.2 V *vs*. Ag/AgCl for 2 h) showed a somewhat regained intensity of the MLCT band at 497 nm (Fig. S9) that is characteristic for the original complex. This suggests that after electrolysis $[Fe(PBI)_3]^{2+}$ can be re-formed to some extent, which may appear surprising considering the presence of Fe(III) in the surface layer. On the other hand, as it was discussed earlier, in the added layer only a part of the solid complex is expected to be in contact with both the electrode support and the solvent, which is necessary to trigger catalysis. Another part remains aqua-coordinated Fe(II) that is capable of accepting the added PBI ligand, and this puts our observations into a complementary relation. The CV scan of the re-dissolved sample also confirms that during electrolysis the majority of the complex remains in a form that reproduces the electrochemical features of the original complex in acetonitrile (Fig. 9b, inset).

Complex **2** shows a vastly different electrochemical behavior in drop-casted samples prepared analogously to **1**/ITO samples. This is not surprising, if one regards the instability of **2** toward hydrolysis in water/acetonitrile. The SEM pictures show a compact layer of the solid complex on ITO (Fig. S10a, insets). The elemental composition by EDX reflects the expected C, N, Fe, F, O and S from the complex with coordinated triflate anions (Fig. S10a). CV scans with **2**/ITO working electrodes, which contain increasing loads of the complex spread over 1.0(1) cm^2 area exhibit lowering currents in the high positive potential range (Fig. S11), which can be attributed to an insulating effect of the non-porous deposit, as clear from the SEM pictures of a used **2**/ITO sample (Fig. S10b, insets). In the CV scans the features indicate mineralization to iron oxide [61] that is also supported by the EDX spectrum, which shows predominantly O and Fe on the surface and only very low presence of N and C, in sharp contrast with the as-prepared **2**/ITO (Fig. S10). The dominance of mineralization is also underlined by XPS (Figs. S7 and S8, Tables S1 and S2), which detected increased Fe and O atomic ratio on the surface, and significantly lowered atomic ratio for C and N. Importantly, both EDX and XPS detected B and Na in the used sample that seem to be participating elements in the oxide material. Note that the **2**/ITO working electrode also produced oxygen. However, the impermeable deposit peeled off from ITO and its physical durability was poor (Fig. S10b shows SEM-EDX analysis results after only 30 min of CPE at +1.2 V *vs*. Ag/AgCl), moreover, the solid could not be re-dissolved in acetonitrile. These findings underline again that **2** (along with its oxidized derivatives) is not a molecular catalyst of water oxidation.

4. Conclusions

Non-symmetric, bidentate heterocyclic ligands were utilized in two Fe(II) complexes, **1** and **2** (Fig. 1) that have been compared in electrocatalytic water oxidation as putative catalysts. Two labile coordination sites at *cis*-positions have been demonstrated earlier to favor small molecule binding and transformation in the presence of the NN' ligands. In this study we focused on the electrochemical behavior of the complexes in (*i*) homogeneous water/acetonitrile mixtures to reveal their intrinsic molecular properties and (*ii*) deposited to ITO as model electrode in order to apply them as heterogenized water oxidation catalyst. The water-insolubility of the complexes seems to be a viable strategy for the design of new molecular catalyst/(photo)anode hybrids. In addition, our study points out that the exchange of a non-coordinated O-atom in the ligand heterocycle (complex **2**) to an NH group (complex **1**) can induce fundamental changes in the redox behavior both in the homogeneous water/acetonitrile phase and when the complexes are deposited to the electrode and tested as water oxidation catalysts in aqueous borate buffer (note that similar results were obtained in carbonate). In addition to the hydrolytic instability of **2** in the presence of water that does not afflict complex **1** this can be attributed to the electron withdrawing nature of O in PBO compared with NH in PBI, which makes PBI capable of supporting the higher oxidation states. As a result, **1**, deposited as a solid on ITO (in contrast to **2**) is suitable for longer term electrocatalysis to produce O_2, without noticeable decomposition of the catalyst layer. Our results underline that the molecular architecture of catalysts designed to fabricate hybrid (photo)electrodes may have two-way effect, *i.e.*, control of the complex stability in the course of catalysis and its strong attachment to the surface by secondary interactions.

Declaration of Competing Interest

The authors declare that they have no known competing financial interests or personal relationships that could have appeared to influence the work reported in this paper.

Acknowledgements

This work is financed by the NKFI-128841 grant, and the VEKOP-2.3.2-16-2016-00011 grant supported by the European Structural and Investment Funds. J. S. Pap is grateful for the J. Bolyai Research Scholarship from the Hungarian Academy of Sciences.

Appendix A. Supplementary material

Supplementary data to this article can be found online at https://doi.org/10.1016/j.jcat.2019.12.003.

References

[1] M.D. Kärkäs, E.V. Johnston, O. Verho, B. Åkermark, Artificial photosynthesis: from nanosecond electron transfer to catalytic water oxidation, Acc. Chem. Res. 47 (2014) 100–111, https://doi.org/10.1021/ar400076j.
[2] J. Chow, Energy resources and global development, Science 302 (2003) 1528–1531, https://doi.org/10.1126/science.1091939.
[3] V. Balzani, A. Credi, M. Venturi, Photochemical conversion of solar energy, ChemSusChem 1 (2008) 26–58, https://doi.org/10.1002/cssc.200700087.

[4] S.I. Allakhverdiev, J.J. Casal, T. Nagata, Photosynthesis from molecular perspectives: towards future energy production, Photochem. Photobiol. Sci. 8 (2009) 137, https://doi.org/10.1039/b823060a.
[5] Y. Tachibana, L. Vayssieres, J.R. Durrant, Artificial photosynthesis for solar water-splitting, Nat. Photonics 6 (2012) 511–518, https://doi.org/10.1038/nphoton.2012.175.
[6] B. Zhang, L. Sun, Artificial photosynthesis: opportunities and challenges of molecular catalysts, Chem. Soc. Rev. 48 (2019) 2216–2264, https://doi.org/10.1039/C8CS00897C.
[7] H.B. Gray, Powering the planet with solar fuel, Nat. Chem. 1 (2009) 7, https://doi.org/10.1038/nchem.141.
[8] A.J. Bard, M.A. Fox, Artificial photosynthesis: solar splitting of water to hydrogen and oxygen, Acc. Chem. Res. 28 (1995) 141–145, https://doi.org/10.1021/ar00051a007.
[9] J.D. Blakemore, R.H. Crabtree, G.W. Brudvig, Molecular catalysts for water oxidation, Chem. Rev. 115 (2015) 12974–13005, https://doi.org/10.1021/acs.chemrev.5b00122.
[10] L. Wu, M. Eberhart, A. Nayak, M.K. Brennaman, B. Shan, T.J. Meyer, A molecular silane-derivatized Ru(II) catalyst for photoelectrochemical water oxidation, J. Am. Chem. Soc. 140 (2018) 15062–15069, https://doi.org/10.1021/jacs.8b10132.
[11] R. Matheu, M.Z. Ertem, C. Gimbert-Suriñach, X. Sala, A. Llobet, Seven coordinated molecular ruthenium-water oxidation catalysts: a coordination chemistry journey, Chem. Rev. (2019), https://doi.org/10.1021/acs.chemrev.8b00537.
[12] M.-P. Santoni, G. La Ganga, V. Mollica Nardo, M. Natali, F. Puntoriero, F. Scandola, S. Campagna, The use of a vanadium species as a catalyst in photoinduced water oxidation, J. Am. Chem. Soc. 136 (2014) 8189–8192, https://doi.org/10.1021/ja5040182.
[13] B. Schwarz, J. Forster, M.K. Goetz, D. Yücel, C. Berger, T. Jacob, C. Streb, Visible-light-driven water oxidation by a molecular manganese vanadium oxide cluster, Angew. Chem. Int. Ed. 55 (2016) 6329–6333, https://doi.org/10.1002/anie.201601799.
[14] M. Okamura, M. Kondo, R. Kuga, Y. Kurashige, T. Yanai, S. Hayami, V.K.K. Praneeth, M. Yoshida, K. Yoneda, S. Kawata, S. Masaoka, A pentanuclear iron catalyst designed for water oxidation, Nature 530 (2016) 465–468, https://doi.org/10.1038/nature16529.
[15] J.L. Fillol, Z. Codolà, I. Garcia-Bosch, L. Gómez, J.J. Pla, M. Costas, Efficient water oxidation catalysts based on readily available iron coordination complexes, Nat. Chem. 3 (2011) 807–813, https://doi.org/10.1038/nchem.1140.
[16] Z. Codolà, L. Gómez, S.T. Kleespies, L. Que Jr, M. Costas, J. Lloret-Fillol, Evidence for an oxygen evolving iron–oxo–cerium intermediate in iron-catalysed water oxidation, Nat. Commun. 6 (2015) 5865.
[17] W.C. Ellis, N.D. McDaniel, S. Bernhard, T.J. Collins, Fast water oxidation using iron, J. Am. Chem. Soc. 132 (2010) 10990–10991, https://doi.org/10.1021/ja104766z.
[18] C. Panda, J. Debgupta, D. Díaz Díaz, K.K. Singh, S. Sen Gupta, B.B. Dhar, Homogeneous photochemical water oxidation by biuret-modified Fe-TAML: Evidence of Fe^{V}(O) intermediate, J. Am. Chem. Soc. 136 (2014) 12273–12282, https://doi.org/10.1021/ja503753k.
[19] L.D. Wickramasinghe, R. Zhou, R. Zong, P. Vo, K.J. Gagnon, R.P. Thummel, Iron complexes of square planar tetradentate polypyridyl-type ligands as catalysts for water oxidation, J. Am. Chem. Soc. 137 (2015) 13260–13263, https://doi.org/10.1021/jacs.5b08856.
[20] B. Chandra, K.K. Singh, S.S. Gupta, Selective photocatalytic hydroxylation and epoxidation reactions by an iron complex using water as the oxygen source, Chem. Sci. 8 (2017) 7545–7551, https://doi.org/10.1039/c7sc02780j.
[21] D. Hong, S. Mandal, Y. Yamada, Y.-M. Lee, W. Nam, A. Llobet, S. Fukuzumi, Water oxidation catalysis with nonheme iron complexes under acidic and basic conditions: homogeneous or heterogeneous?, Inorg. Chem. 52 (2013) 9522–9531, https://doi.org/10.1021/ic401180r.
[22] B. Das, B.-L. Lee, E.A. Karlsson, T. Åkermark, A. Shatskiy, S. Demeshko, R.-Z. Liao, T.M. Laine, M. Haukka, E. Zeglio, A.F. Abdel-Magied, P.E.M. Siegbahn, F. Meyer, M.D. Kärkäs, E.V. Johnston, E. Nordlander, B. Åkermark, Water oxidation catalyzed by molecular di- and nonanuclear Fe complexes: importance of a proper ligand framework, Dalton Trans. 45 (2016) 13289–13293, https://doi.org/10.1039/C6DT01554A.
[23] C.-F. Leung, S.-M. Ng, C.-C. Ko, W.-L. Man, J. Wu, L. Chen, T.-C. Lau, A cobalt(II) quaterpyridine complex as a visible light-driven catalyst for both water oxidation and reduction, Energy Environ. Sci. 5 (2012) 7903, https://doi.org/10.1039/c2ee21840b.
[24] H. Lei, A. Han, F. Li, M. Zhang, Y. Han, P. Du, W. Lai, R. Cao, Electrochemical, spectroscopic and theoretical studies of a simple bifunctional cobalt corrole catalyst for oxygen evolution and hydrogen production, Phys. Chem. Chem. Phys. 16 (2014) 1883–1893, https://doi.org/10.1039/C3CP54361G.
[25] M.M. Najafpour, H. Feizi, Water oxidation by Ni(1,4,8,11-tetraazacyclotetradecane)$^{2+}$ in the presence of carbonate: new findings and an alternative mechanism, Dalton Trans. 47 (2018) 6519–6527, https://doi.org/10.1039/C8DT00068A.
[26] H. Feizi, R. Bagheri, Z. Jagličić, J.P. Singh, K.H. Chae, Z. Song, M.M. Najafpour, A nickel(II) complex under water-oxidation reaction: what is the true catalyst?, Dalton Trans. 48 (2019) 547–557, https://doi.org/10.1039/C8DT03990A.
[27] Ł. Szyrwiel, D. Lukács, T. Ishikawa, J. Brasun, Ł. Szczukowski, Z. Szewczuk, B. Setner, J.S. Pap, Electrocatalytic water oxidation influenced by the ratio between Cu^{2+} and a multiply branched peptide ligand, Catal. Commun. 122 (2019) 5–9, https://doi.org/10.1016/j.catcom.2019.01.004.
[28] D. Lukács, Ł. Szyrwiel, J. Pap, Copper containing molecular systems in electrocatalytic water oxidation—trends and perspectives, Catalysts 9 (2019) 83, https://doi.org/10.3390/catal9010083.
[29] K.D. Vogiatzis, M.V. Polynski, J.K. Kirkland, J. Townsend, A. Hashemi, C. Liu, E.A. Pidko, Computational approach to molecular catalysis by 3d transition metals: challenges and opportunities, Chem. Rev. 119 (2019) 2453–2523, https://doi.org/10.1021/acs.chemrev.8b00361.
[30] F.T. de Oliveira, A. Chanda, D. Banerjee, X. Shan, S. Mondal, L. Que, E.L. Bominaar, E. Munck, T.J. Collins, Chemical and spectroscopic evidence for an Fe^{V}-oxo complex, Science 315 (2007) 835–838, https://doi.org/10.1126/science.1133417.
[31] Liang-Xian Liu, Recent uses of iron catalysts in organic reactions, Curr. Org. Chem. 14 (2010) 1099–1126, https://doi.org/10.2174/138527210791317094.
[32] W. Nam, High-valent Iron(IV)–oxo complexes of heme and non-heme ligands in oxygenation reactions, Acc. Chem. Res. 40 (2007) 522–531, https://doi.org/10.1021/ar700027f.
[33] J. Hohenberger, K. Ray, K. Meyer, The biology and chemistry of high-valent iron–oxo and iron–nitrido complexes, Nat. Commun. 3 (2012) 720.
[34] M.D. Kärkäs, O. Verho, E.V. Johnston, B. Åkermark, Artificial photosynthesis: molecular systems for catalytic water oxidation, Chem. Rev. 114 (2014) 11863–12001, https://doi.org/10.1021/cr400572f.
[35] M.F. Pinto, B. de P. Cardoso, S. Barroso, A.M. Martins, B. Royo, Chelating bis-N-heterocyclic carbene complexes of iron(II) containing bipyridyl ligands as catalyst precursors for oxidation of alcohols, Dalton Trans. 45 (2016) 13541–13546, https://doi.org/10.1039/C6DT02718K.
[36] A. Singh, L. Spiccia, Water oxidation catalysts based on abundant 1st row transition metals, Coord. Chem. Rev. 257 (2013) 2607–2622, https://doi.org/10.1016/j.ccr.2013.02.027.
[37] Z. Codolà, I. Gamba, F. Acuña-Parés, C. Casadevall, M. Clémancey, J.-M. Latour, J. M. Luis, J. Lloret-Fillol, M. Costas, Design of iron coordination complexes as highly active homogenous water oxidation catalysts by deuteration of oxidation-sensitive sites, J. Am. Chem. Soc. 141 (2019) 323–333, https://doi.org/10.1021/jacs.8b10211.
[38] K.G. Kottrup, D.G.H. Hetterscheid, Evaluation of iron-based electrocatalysts for water oxidation – an on-line mass spectrometry approach, Chem. Commun. 52 (2016) 2643–2646, https://doi.org/10.1039/C5CC10092E.
[39] K.G. Kottrup, S. D'Agostini, P.H. van Langevelde, M.A. Siegler, D.G.H. Hetterscheid, Catalytic activity of an iron-based water oxidation catalyst: substrate effects of graphitic electrodes, ACS Catal. 8 (2018) 1052–1061, https://doi.org/10.1021/acscatal.7b03284.
[40] M.M. Najafpour, A.N. Moghaddam, D.J. Sedigh, M. Hołyńska, A dinuclear iron complex with a single oxo bridge as an efficient water-oxidizing catalyst in the presence of cerium(IV) ammonium nitrate: new findings and current controversies, Catal. Sci. Technol. 4 (2014) 30–33, https://doi.org/10.1039/C3CY00644A.
[41] S. Berardi, S. Drouet, L. Francàs, C. Gimbert-Suriñach, M. Guttentag, C. Richmond, T. Stoll, A. Llobet, Molecular artificial photosynthesis, Chem. Soc. Rev. 43 (2014) 7501–7519, https://doi.org/10.1039/C3CS60405E.
[42] C. Gao, J. Wang, H. Xu, Y. Xiong, Coordination chemistry in the design of heterogeneous photocatalysts, Chem. Soc. Rev. 46 (2017) 2799–2823, https://doi.org/10.1039/C6CS00727A.
[43] S. Bae, J.-E. Jang, H.-W. Lee, J. Ryu, Tailored assembly of molecular water oxidation catalysts on photoelectrodes for artificial photosynthesis: tailored assembly of molecular water oxidation catalysts on photoelectrodes for artificial photosynthesis, Eur. J. Inorg. Chem. (2019), https://doi.org/10.1002/ejic.201801328.
[44] R.H. Crabtree, Resolving heterogeneity problems and impurity artifacts in operationally homogeneous transition metal catalysts, Chem. Rev. 112 (2012) 1536–1554, https://doi.org/10.1021/cr2002905.
[45] V. Artero, M. Fontecave, Solar fuels generation and molecular systems: is it homogeneous or heterogeneous catalysis?, Chem. Soc. Rev. 42 (2013) 2338–2356, https://doi.org/10.1039/C2CS35334B.
[46] M.D. Kärkäs, B. Åkermark, Water oxidation using earth-abundant transition metal catalysts: opportunities and challenges, Dalton Trans. 45 (2016) 14421–14461, https://doi.org/10.1039/C6DT00809G.
[47] T. Shi, H. Li, L. Ding, F. You, L. Ge, Q. Liu, K. Wang, Facile preparation of unsubstituted iron(II) phthalocyanine/carbon nitride nanocomposites: a multipurpose catalyst with reciprocally enhanced photo/electrocatalytic activity, ACS Sust. Chem. Eng. 7 (2019) 3319–3328, https://doi.org/10.1021/acssuschemeng.8b05366.
[48] E.L. Demeter, S.L. Hilburg, N.R. Washburn, T.J. Collins, J.R. Kitchin, Electrocatalytic oxygen evolution with an immobilized TAML activator, J. Am. Chem. Soc. 136 (2014) 5603–5606, https://doi.org/10.1021/ja5015986.
[49] J.S. Pap, A. Draksharapu, M. Giorgi, W.R. Browne, J. Kaizer, G. Speier, Stabilisation of μ-peroxido-bridged Fe(III) intermediates with non-symmetric bidentate N-donor ligands, Chem. Commun. 50 (2014) 1326–1329, https://doi.org/10.1039/C3CC48196D.
[50] H.-L. Xia, S. Ardo, A.A. Narducci Sarjeant, S. Huang, G.J. Meyer, Photodriven spin change of Fe(II) benzimidazole compounds anchored to nanocrystalline TiO_2 thin films, Langmuir 25 (2009) 13641–13652, https://doi.org/10.1021/la9022213.
[51] W.A. Hoffert, M.T. Mock, A.M. Appel, J.Y. Yang, Incorporation of hydrogen-bonding functionalities into the second coordination sphere of iron-based water-oxidation catalysts, Eur. J. Inorg. Chem. 2013 (2013) 3846–3857, https://doi.org/10.1002/ejic.201201499.

[52] M.J. Collins, K. Ray, L. Que, Electrochemical generation of a nonheme oxoiron (IV) complex, Inorg. Chem. 45 (2006) 8009–8011, https://doi.org/10.1021/ic061263i.
[53] Z. Codolà, I. Garcia-Bosch, F. Acuña-Parés, I. Prat, J.M. Luis, M. Costas, J. Lloret-Fillol, Electronic effects on single-site iron catalysts for water oxidation, Chem. - Eur. J. 19 (2013) 8042–8047, https://doi.org/10.1002/chem.201301112.
[54] F. Acuña-Parés, Z. Codolà, M. Costas, J.M. Luis, J. Lloret-Fillol, unraveling the mechanism of water oxidation catalyzed by nonheme iron complexes, Chem. - Eur. J. 20 (2014) 5696–5707, https://doi.org/10.1002/chem.201304367.
[55] E.S. Rountree, B.D. McCarthy, T.T. Eisenhart, J.L. Dempsey, Evaluation of homogeneous electrocatalysts by cyclic voltammetry, Inorg. Chem. 53 (2014) 9983–10002, https://doi.org/10.1021/ic500658x.
[56] M.K. Coggins, M.-T. Zhang, A.K. Vannucci, C.J. Dares, T.J. Meyer, Electrocatalytic water oxidation by a monomeric amidate-ligated Fe(III)–aqua complex, J. Am. Chem. Soc. 136 (2014) 5531–5534, https://doi.org/10.1021/ja412822u.
[57] D.R. Weinberg, C.J. Gagliardi, J.F. Hull, C.F. Murphy, C.A. Kent, B.C. Westlake, A. Paul, D.H. Ess, D.G. McCafferty, T.J. Meyer, Proton-coupled electron transfer, Chem. Rev. 112 (2012) 4016–4093, https://doi.org/10.1021/cr200177j.
[58] E.C. Ellingsworth, B. Turner, G. Szulczewski, Thermal conversion of $[Fe(phen)_3](SCN)_2$ thin films into the spin crossover complex $Fe(phen)_2(NCS)_2$, RSC Adv. 3 (2013) 3745, https://doi.org/10.1039/c3ra22534h.
[59] L. Li, A.R. Craze, R. Akiyoshi, A. Tsukiashi, S. Hayami, O. Mustonen, M.M. Bhadbhade, S. Bhattacharyya, C.E. Marjo, Y. Wang, L.F. Lindoy, J.R. Aldrich-Wright, F. Li, Direct monitoring of spin transitions in a dinuclear triple-stranded helicate iron(II) complex through X-ray photoelectron spectroscopy, Dalton Trans. 47 (2018) 2543–2548, https://doi.org/10.1039/C7DT04190J.
[60] A. Pronschinske, R.C. Bruce, G. Lewis, Y. Chen, A. Calzolari, M. Buongiorno-Nardelli, D.A. Shultz, W. You, D.B. Dougherty, Iron(II) spin crossover films on Au(111): scanning probe microscopy and photoelectron spectroscopy, Chem. Commun. 49 (2013) 10446, https://doi.org/10.1039/c3cc44904a.
[61] H. Bülter, G. Denuault, S. Mátéfi-Tempfli, M. Mátéfi-Tempfli, C. Dosche, G. Wittstock, Electrochemical analysis of nanostructured iron oxides using cyclic voltammetry and scanning electrochemical microscopy, Electrochim. Acta 222 (2016) 1326–1334, https://doi.org/10.1016/j.electacta.2016.11.108.